μSR relaxation functions in magnetic materials

Y J Uemura

Columbia University, USA

1 Introduction

As a point-like magnetic probe in real space, spin relaxation of positive muons in solids is subject to essentially the same processes as for the case of nuclear magnetic resonance (NMR) or electron spin resonance (ESR). Unlike NMR and ESR in frequency space, however, muon spin relaxation (μSR) probes spin relaxation in time space. Unlike NMR and ESR measurements performed mostly in high magnetic fields and resonating RF field, the time evolution of muon spins in μSR can be observed even in zero magnetic field thanks to the radioactive decay of the spin probe. These unique features of μSR provide opportunities for illustrating and illuminating basic principles of spin relaxation processes in a way different from descriptions in standard NMR textbooks (Abragam 1961, Slichter 1963, Jaccarino 1965).

This article provides an overview of muon spin relaxation functions with examples of experimental data and some remarks on historical developments. We start with the static random local field, and examine the cases of well-defined unique local field(s), Gaussian and Lorentzian random fields, as well as a field distribution expected for incommensurate spin density wave and perturbed spin-gap systems. We then proceed to the relaxation functions in fluctuating dynamic random local fields, with examples of μSR studies in MnSi and dilute-alloy spin glass systems. We will also consider the origin of powered exponential relaxation functions observed in spin glass and manganate systems.

2 Static relaxation functions

2.1 Field distribution

After being implanted into the specimen, a positive muon loses its kinetic energy by ionising outer-shell electrons near its trajectory, and finally stops usually at an interstitial site. Fortunately, this stopping process does not involve a magnetic interaction, and

occurs in a very short time, typically much less than 1ns (Brewer *et al.* 1975). Each muon spin at an interstitial site therefore starts its time evolution with an initial spin polarisation of 100%. The average spin polarisation of muon spins at a time t after the implantation of muons is defined as the muon spin relaxation function $G(t)$. The typical time window for observing $G(t)$ in μSR is from $t \sim 10$ ns to $t \sim 10\mu$s. In this section, we assume that each muon remains stationary after stopping at an interstitial site: *i.e.* no muon diffusion. We also assume that muons exist without having bound electrons: *i.e.* no muonium formation.

The local internal magnetic field at a muon site originates from a dipolar interaction with surrounding nuclear or electronic spins, as well as contact hyperfine fields from the spin density at the muon site. The internal field from spins in the long-range ordered state of regular ferro- or antiferromagnets often tends to be unique in magnitude with a particular direction with respect to the crystal lattice. Multiple muon sites in a unit cell, or crystallographically equivalent but magnetically inequivalent muon sites could result in multiple magnitudes of such field. When the direction of surrounding moments is random, as in the case of nuclear dipolar fields or in the frozen state of spin glasses, the local field has a continuous distribution. Let us express the probability distribution function of the internal magnetic field H as $P(H_i)$ $(i = x, y, z)$ and $P(|H|)$ where $|H|$ stands for the magnitude of the field.

Nuclear dipolar fields often originate from several static nuclear moments, having random orientation with each other, located at approximately the same distance from the muon site. As a vector some of the field from these nuclear moments, the internal field in this case, can be well approximated by a Gaussian distribution

$$P^G(H_i) = \frac{\gamma_\mu}{\sqrt{2\pi}\Delta} \times \exp(-\gamma_\mu^2 H_i^2/2\Delta^2) \quad (i = x, y, z), \tag{1a}$$

$$P^G(|H|) = \left(\frac{\gamma_\mu}{\sqrt{2\pi}\Delta}\right)^3 \times \exp(-\gamma_\mu^2 |H|^2/2\Delta^2) \times 4\pi|H|^2, \tag{1b}$$

where γ_μ is the gyromagnetic ratio 13.554×2π kHz/G of positive muon. Note that the probability for H_i is centered around zero, while that for $|H|$ has a maximum at a finite value of Δ. A Gaussian is a very good approximation for a binomial distribution with multiplicity n of more than $\sim$ 3-4. This distribution can then be expected when the random field originates effectively from several sources in concentrated spin systems. Even when the field is due to a single moment near the muon site, randomness of the moment direction results in $|H|$ for dipolar field ranging between a minimum value $|H|_{\rm min}$ and the maximum value $|H|_{\rm max}$=2$|H|_{\rm min}$. The variable range of $|H|$ then becomes somewhat similar to that of $P^G(|H|)$. A Gaussian distribution therefore often works well for describing a variable range of random local fields at a muon site.

In contrast, in dilute spin systems such as dilute-alloy spin glasses, one would expect a Lorentzian distribution

$$P^L(H_i) = \frac{\gamma_\mu}{\pi} \times \frac{a}{a^2 + \gamma_\mu^2 H_i^2}, \quad (i = x, y, z), \tag{2a}$$

$$P^L(|H|) = \frac{\gamma_\mu^3}{\pi^2} \times \left[\frac{a}{a^2 + \gamma_\mu^2 |H|^2}\right]^2 \times 4\pi|H|^2. \tag{2b}$$

In the dilute limit, a Lorentzian is the exact distribution for spin systems producing local fields with a $1/r^3$ interaction, where r denotes the distance between the moment and the muon site. In this limit, the amplitude parameter a is proportional to the number density (*i.e.* concentration) of the moments (Luke *et al.* 1998). In spatially dilute spin systems, different muon sites are in different surrounding moment configurations: some having nearby moments and others without any. The local field therefore has a much wider variety than the Gaussian case: this situation is well represented by a Lorentzian.

2.2 Relaxation functions in ZF and LF

Figure 1 shows a schematic view of μSR apparatus for zero-field (ZF), longitudinal-field

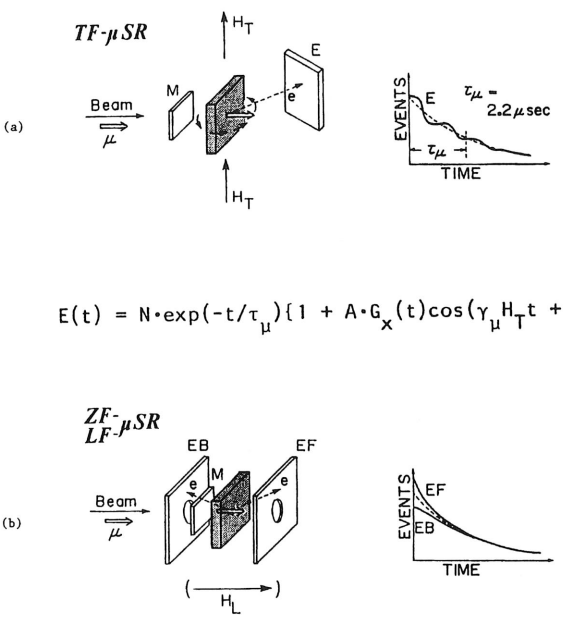

Figure 1. *A schematic view of experimental methods of (a) transverse-field (TF) μSR and (b) zero- and longitudinal-field (ZF and LF) μSR. An incoming polarised muon is identified by M counter, and stopped in a specimen (dotted piece). Decay positrons are detected by counters E, EF, and EB, and the measured time spectra reflect muon spin polarisation in the way as shown in the figure.*

(LF) and transverse-field (TF) configurations. We denote the direction of initial muon spin polarisation as $\hat{\mathbf{z}}$. The muon spin precesses around the local magnetic field H, as illustrated in Figure 2. Then the z component of the spin polarisation $\sigma_z(t)$ is given as

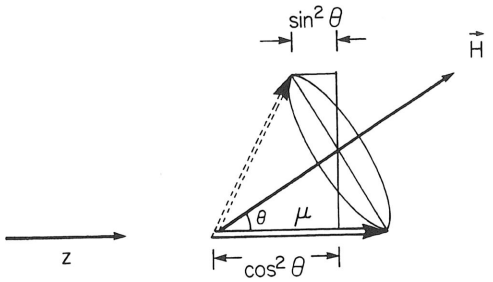

Figure 2. *Muon spin precession around the internal magnetic field H. θ denotes the angle between initial muon spin polarisation direction $\hat{\mathbf{z}}$ and* **H**. *The z-component of the spin polarisation σ_z has a time-independent component proportional to* $\cos^2\theta$, *while* $\sin^2\theta$ *shows precession with the frequency* $\gamma_\mu|H|$.

$$\sigma_z(t) = \cos^2\theta + \sin^2\theta\,\cos(\gamma_\mu|H|t), \tag{3}$$

where the first term corresponds to the average time-independent polarisation along the z component while the second term to the precessing asymmetry. The muon spin relaxation function $G_z(t)$ can be obtained by averaging $\sigma_z(t)$ over the field distribution function $P(H)$. In the following, we discuss the case for powder/ceramic specimens, where the direction of H is random and isotropic.

For a unique magnitude of $|H|$, the directional average will lead Equation 3 to the relaxation function

$$G_z(t) = \frac{1}{3} + \left(\frac{2}{3}\right)\cos(\gamma_\mu|H|t). \tag{4}$$

Figure 3 shows a ZF-μSR result observed in an antiferromagnet CaV_3O_7 (Luke *et al.* 1998). Here we see a beat of two precession frequencies within the 2/3 component, in addition to the non-precessing 1/3 component. The frequency of this precession is proportional to the sub-lattice magnetisation of V moments. μSR measurements in the ordered state of ferro or antiferromagnets have been performed since the 1970's, in Fe (Nishida *et al.* 1977), Ni (Foy *et al.* 1973), Fe_2O_3 (Graf *et al.* 1978), La_2CuO_4 (Uemura *et al.* 1987), and many other systems.

Extensive studies of ZF- and LF-μSR started at TRIUMF in 1978 (Hayano *et al.* 1978a, Hayano *et al.* 1978b, Uemura *et al.* 1979, Hayano *et al.* 1979) . Figure 4 shows the first ZF- and LF-μSR spectra due to nuclear dipolar fields observed in MnSi (Hayano *et al.* 1978b) at room temperature, where the muon spin is depolarised by nuclear dipolar fields from surrounding Mn nuclei. The zero-field relaxation function for this case can be obtained by averaging Equation 3 over the Gaussian distribution $P^G(H)$, leading to

$$G_z(t) = \frac{1}{3} + \frac{2}{3}(1 - \Delta^2 t^2)\exp(-\Delta^2 t^2/2), \tag{5}$$

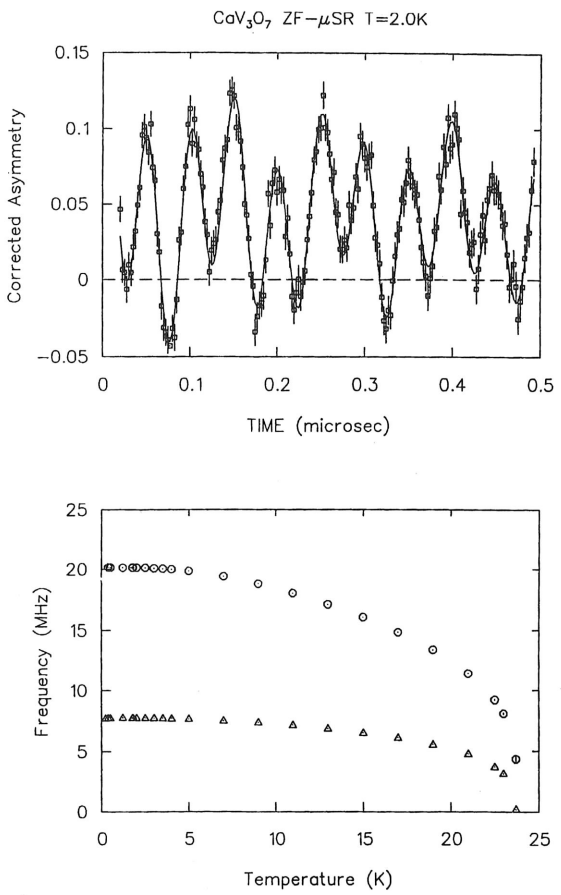

Figure 3. *(a) Zero-field μSR spectra observed in an antiferromagnet CaV_3O_7 at $T = 2K$. We see precession signals with two distinct frequencies plus the 1/3 non-precessing asymmetry. (b) Temperature dependence of the observed two frequencies in CaV_3O_7 (Walstedt and Walker 1974).*

which is known as the Kubo-Toyabe function derived first in 1966 (Kubo and Toyabe 1967). This function has a persisting 1/3 asymmetry and the 2/3 component showing a damped oscillation around $|H|$. The width Δ of random fields can be estimated from the rate of the damped oscillation. In MnSi, the average local field Δ/γ_μ is about 4G.

Application of a longitudinal field parallel to $\hat{\mathbf{z}}$ helps aligning the local field along the z axis. The LF relaxation function for a Gaussian local field becomes (Hayano *et al.* 1979, Kubo and Toyabe 1967)

$$G_z^G(t, H_L) = 1 - \left(\frac{2\Delta^2}{\omega_L^2}\right)\left[1 - e^{-\Delta^2 t^2/2}\cos(\omega_L t)\right] + \left(\frac{2\Delta^4}{\omega_L^3}\right)\int_0^t e^{-\Delta^2 t^2/2}\sin(\omega_L \tau)d\tau, \quad (6)$$

where H_L stands for the applied longitudinal field and $\omega_L = \gamma_\mu H_L$. The second and

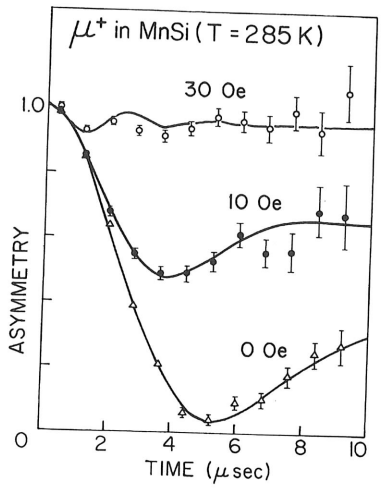

Figure 4. *ZF- and LF-μSR spectra observed in MnSi at room temperature. At this temperature, muon spins are depolarised by nuclear dipolar fields. The ZF spectrum represents the first observation of "Kubo-Toyabe" function (Hayano 1978a).*

the third terms of Equation 6 become vanishingly small for $\Delta/\omega_L \to 0$. For a fixed value of $|H|$ with an applied LF of $H_L = |H|$, the powder average of the $\cos^2$ term in Equation 3 becomes 1/2. This implies that the magnitude Δ of the static random field is approximately comparable to the value of ω_L which restores the 1/3 component to 1/2. Thus, the LF measurements provide an independent way to estimate Δ. The restoration of the persisting asymmetry in LF is usually called "decoupling". Note that the initial oscillation in the H_L = 30G data in Figure 4 has the frequency of ω_L, originating from the second term of Equation 6.

In a Lorentzian local field, the ZF relaxation function is given as (Kubo 1981,Uemura *et al.* 1980)

$$G_z^L(t) = \frac{1}{3} + \frac{2}{3}(1 - at)\exp(-at). \tag{7}$$

This function has a shallower "dip" of the damped oscillation compared to the Gaussian Kubo-Toyabe function in Equation 5, corresponding to a faster damping due to a wider range of $|H|$. The LF relaxation function in Lorentzian fields becomes (Uemura *et al.* 1981, Uemura *et al.* 1985)

$$G_z^L(t, H_L) = 1 - (a/\omega_L)j_1(\omega_L t)\exp(-at) - (a/\omega_L)^2[j_0(\omega_L t)\exp(-at) - 1]$$
$$- [1 + (a/\omega_L)^2]a\int_0^t j_0(\omega_L \tau)\exp(-a\tau)d\tau, \tag{8}$$

where j_0 and j_1 denote spherical Bessel functions. Figure 5 shows ZF- and LF-μSR results, together with fits to Equation 7 and Equation 8, obtained in a dilute alloy spin glass CuMn (Mn 1 at.%) at T = 5K which is approximately a half of the spin-freezing temperature T_g=10.8K (Uemura *et al.* 1981). Independent estimates for the field amplitude parameter a from ZF and LF studies agree rather well, as shown in Figure 6 (Uemura *et al.* 1985). In Figure 7, we plot Equation 8 for several values of ω_L/a.

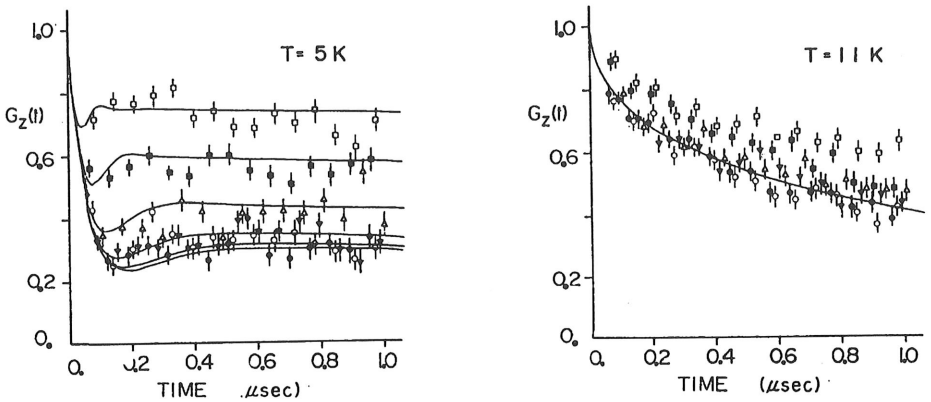

Figure 5. *ZF- and LF-μSR spectra observed in a spin glass CuMn (1.1 at.% Mn, T_g = 10.8K) at (a) T = 5K and (b) T = 11K. The results in (a) exhibit line shapes of almost static relaxation functions for Lorentzian local fields in Equation 7 and Equation 8, while (b) show only a small field dependence, characteristic of relaxation due to fluctuating dynamic local fields (Uemura* et al. *1981).*

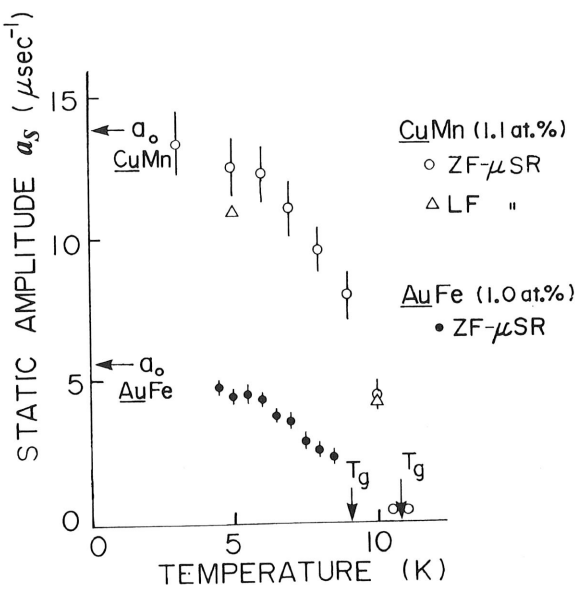

Figure 6. *Temperature dependence of the static field parameter a_s observed in CuMn (1.1 at.%) in ZF- and LF-μSR, and in AuFe (1.0 at.%) in ZF-μSR. The ZF and LF results show a reasonable agreement. The low temperature results extrapolate well towards theoretical values a_0 calculated from the size of frozen moment and its concentration (Uemura* et al. *1985).*

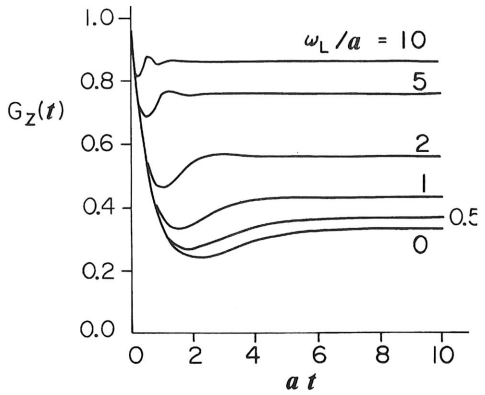

Figure 7. *The LF relaxation functions for Lorentzian local fields, Equation 8, plotted for selected values of* ω_L/a *(Uemura* et al. *1985).*

2.3 Relaxation functions in TF

In a high transverse field H_T, applied parallel to $\hat{\mathbf{x}}$, the muon spin precesses around the local field obtained by a vector sum of H_T and H. Suppose H has a Gaussian distribution Equation 1. For $H_T \gg \Delta/\gamma_\mu$, the direction of local field is almost parallel to TF. Its magnitude is given approximately by $|H_T| \pm |H_i|$ with only one (projection) component such as $i = x$. Thus the precessing asymmetry is given as

$$A(t) = \cos(\omega_T t) \exp(-\Delta^2 t^2/2), \tag{9}$$

or equivalently

$$G_x^G(t) = \exp(-\Delta^2 t^2/2). \tag{10}$$

The TF relaxation function $G_x^G(t)$ does not depend on H_T as long as $H_T \gg \Delta/\gamma_\mu$. At early times $\Delta t \ll 1$, the Kubo-Toyabe function in ZF decays as $(1 - \Delta^2 t^2)$. Compared to this the TF relaxation function in Equation 10 has only a half decay rate, with the initial decay of $(1 - \Delta^2 t^2/2)$. This is because the ZF relaxation reflects x and y components of random local fields while the TF relaxation is due to only one such component.

There exists another difference between ZF and TF. In a high TF, static nuclear moments would precess around the TF. If this precession is fast enough, it would average out y and z components of the moment, effectively reducing Δ. Together with the above mentioned factor of 2 difference in the decay late, this quenching of the "non-secular term" of dipolar interactions in TF would make the decay rate Δ^2 apparently smaller by a factor of 5 as compared to ZF. This feature has been demonstrated by μSR in ZrH_2 (Uemura *et al.* 1979), as shown in Figure 8.

2.4 Generalisation

Though he did not publish the results, Kubo developed more general arguments about relaxation functions Yamazaki (1997). One starts with the transverse relaxation function $G_x(t)$. The Gaussian case is given in Equation 10, while the Lorentzian case obviously

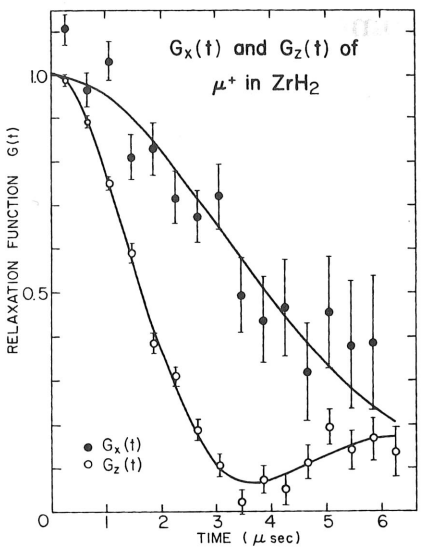

Figure 8. *Comparison of ZF relaxation function $G_z(t)$ and TF relaxation function $G_x(t)$ observed by μ^+ in ZrH_2 at room temperature. The effective decay rate Δ^2 of the polarisation in ZF and LF exhibits a factor of 5 difference, due to the contribution of non-secular term of dipolar interaction in ZF (Uemura* et al. *1979).*

becomes $G_x^L(t) = \exp(-at)$. Kubo gave the zero-field functions as

$$G_z(t) = \frac{1}{3} + \frac{2}{3}\frac{d}{dt}[t\,G_x(t)], \tag{11}$$

which we might call Kubo's golden formula. Indeed, this leads to Equation 5 for the Gaussian and Equation 7 for Lorentzian distribution. When we notice that $G_x(t)$ in these cases can be given by $G_x(t) = \exp[-(\lambda t)^\alpha/\alpha]$ with $\alpha = 2$ for a Gaussian and 1 for a Lorentzian, we can then obtain cases interpolating between Gaussian and Lorentzian with a general stretching exponent $1 < \alpha < 2$. Here the ZF relaxation function becomes (Crook and Cywinski 1997)

$$G_z(t) = \frac{1}{3} + \frac{2}{3}[1 - (\lambda t)^\alpha]\exp[-(\lambda t)^\alpha/\alpha], \tag{12}$$

The field distribution corresponding to this form is called a Lévy distribution (Shlesiger *et al.* 1995). This formula is useful in fitting data obtained in spin glass systems with medium range of concentration.

Kubo also contributed a general formula to obtain LF relaxation functions as

$$G_z(t) = 1 - 2Q(t)\,t\left[\frac{\cos(\omega_L t)}{\omega_L^2 t^2}\right] + \frac{2}{\omega_L^2}\left[\frac{Q(t)}{t}\right]_{t=0} + 2\int_0^t \frac{j_0(\omega_L \tau)}{\omega_L^2}\left[\frac{Q(\tau)}{\tau}\right]' d\tau, \tag{13}$$

where Q(t) stands for $(d/dt)G_x(t)$ and $j_0(t)$ for $\sin(t)/t$. Here the third term exists to compensate divergence of the second term at $t = 0$.

3 Spatially inhomogeneous spin density

Spin density waves have sinusoidal amplitude modulation of spin density at position r. Suppose (a) the local field at a position r in real space is proportional to the spin density $\rho(r)$, as in a predominantly contact hyperfine interaction, and (b) the period of modulation is incommensurate with the lattice period. Then crystalographically equivalent muon sites will be attached to various different magnitudes of local fields corresponding to different phases of the sinusoidal modulation. The probability to find a field $H(r) = H_{\max}\cos(r)$ is proportional to $1/\sin(r)$, so the field distribution becomes (Le *et al.* 1993)

$$P^{\rm sdw}(|H|) \propto [1 - (|H|/H_{\max})^2]^{-1/2}. \tag{14}$$

Fourier transform of this field distribution is a Bessel function and the zero-field relaxation function is given as

$$G_z(t) = \frac{1}{3} + \frac{2}{3} j_0(\gamma_\mu H_{\max} t). \tag{15}$$

If there is some broadening of the distribution, e.g., by nuclear dipolar fields, the Bessel function will exhibit a slow damping.

This relaxation function was first observed (Le *et al.* 1993) in a typical incommensurate spin density wave system $(TMTSF)_2PF_6$, as shown in Figure 9. Subsequently, a similar

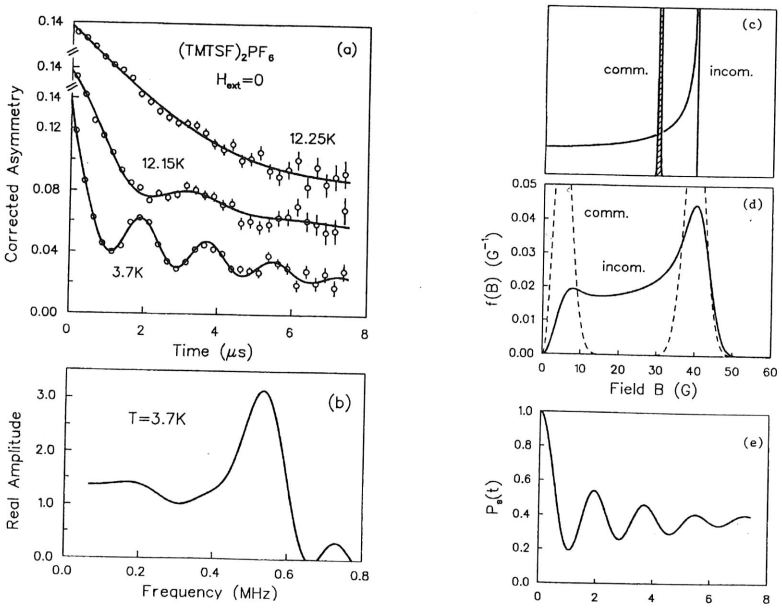

Figure 9. *(a) Muon spin relaxation function, and (b) the field distribution observed in ZF-μSR in an organic conductor $(TMTSF)_2$-PF_6 which has incommensurate spin density wave state below $T = 12.2K$. (c) shows the expected field distribution for the ICSDW state (Equation 14) compared to the case of commensurate modulation. The expected actual field distribution (d) results in Bessel function (Equation 15) associated with a slow damping (e) (Le* et al. *1993).*

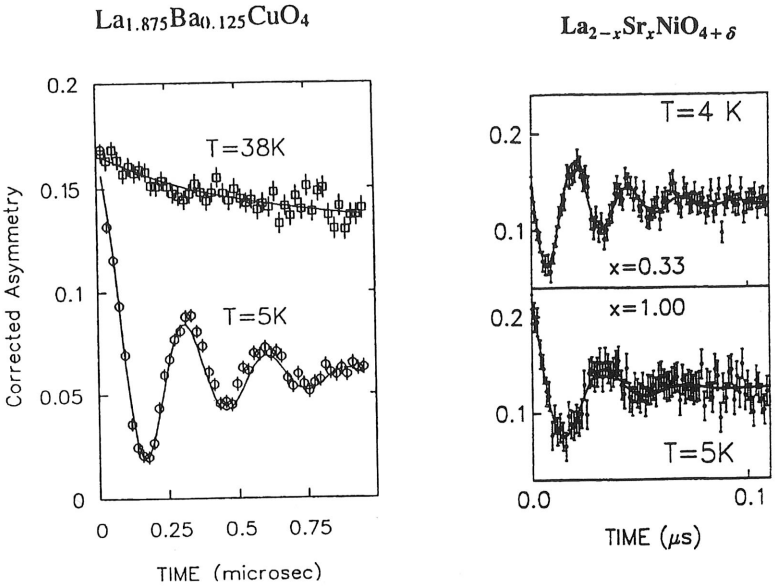

Figure 10. *ZF-μSR spectrum observed in (a) $La_{1.875}Ba_{0.125}CuO_4$ (Luke* et al. *1998) compared with those in (b) $La_{2-x}Sr_xNiO_4$ (Chow* et al. *1996). (a) shows a faster damping close to Bessel function expected for the ICSDW modulation, while (b) shows much slower damping, possibly related to locally more commensurate spin structure in the charge/spin stripe modulation.*

line shape was observed in $HoNi_2B_2C$ (Le *et al.* 1997), UNi_2Al_3 (Uemura *et al.* 1993), and in $La_{1.875}Ba_{0.125}CuO_4$ (Luke *et al.* 1998), as shown in Figure 10. $La_{1.875}Ba_{0.125}CuO_4$ is related to possible charge/spin stripe formation of the cuprate near the 1/8 hole concentration. In locally commensurate stripe modulation, however, one would expect a lineshape with slower damping, as observed in $(La,Sr)_2NiO_4$ (Chow *et al.* 1996) (see Figure 10). The observed Bessel function line shape in $La_{1.875}Ba_{0.125}CuO_4$ may therefore indicate that the spin structure of the 1/8 La214 systems is closer to incommensurate spin density waves.

$CuGeO_3$ has a quasi 1-dimensional linear chain of S=1/2 Cu moments coupled with antiferromagnetic exchange interaction along the chain direction. This system shows a spin Peierls transition at $T \sim 15$K (Hase *et al.* 1993b) with non-magnetic spin-singlet ground state, as was confirmed by μSR measurements (Kojima *et al.* 1997) shown in Figure 11. Substitution of very small amount of Cu with Zn results in antiferromagnetic long-range order of the Cu moments (Hase *et al.* 1993a,Manabe *et al.* 1998). Fukuyama *et al.* (1996) presented a picture that the size of the ordered Cu moment varies with respect to the distance from a Zn impurity, as illustrated in Figure 12, in a region of low Zn concentration (typically less than a few percent). Lattice distortion around an impurity locally suppresses the spin Peierls dimerisation, inducing large ordered moment, while the tendency towards singlet formation is stronger for Cu moments distant from the impurity site.

Kojima *et al.* (1997) calculated the local field distribution and the ZF muon spin re-

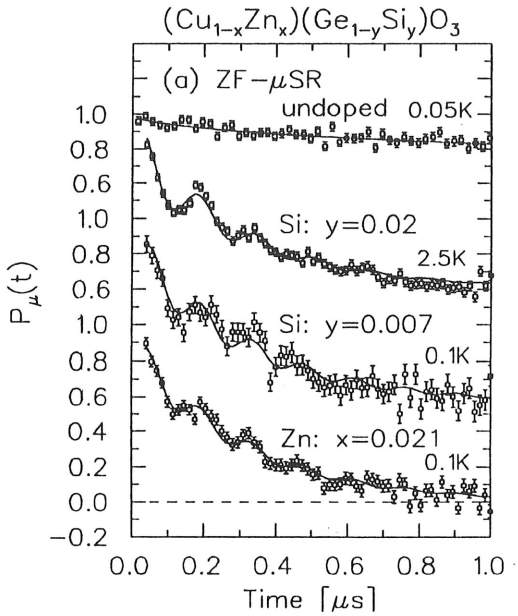

Figure 11. *ZF-μSR spectra observed in pure and Zn-substituted $CuGeO_3$. The results for the pure system confirm non-magnetic singlet ground state of the spin-Peierls system $CuGeO_3$, while the results from Zn-doped system exhibit characteristic features expected for a spatially inhomogeneous ordered moment size. (Kojimma* et al. *1997).*

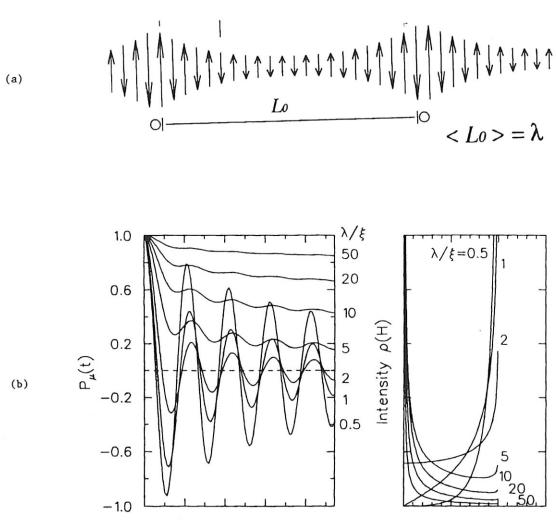

Figure 12. *Illustration of (a) spatially inhomogeneous ordered moment size in the long-range ordered antiferromagnetic state coexisting with dimerisation, proposed by Fukuyama et al. (1978), and (b) corresponding ZF-μSR relaxation functions and field distributions in Zn-substituted $CuGeO_3$ (Kojima 1997,Fukuyama 1996).*

laxation function, shown in Figure 12, corresponding to this situation. The μSR lineshape observed in Zn 2.1% $CuGeO_3$ in Figure 11 shows characteristic features of this line shape. When such a relaxation function is fitted with a simple frequency and a relaxation rate, the phase of the cosine oscillation at $t = 0$ shows an apparent deviation from 0 (Kojima *et al.* 1997), as was found in the observed data. Thus, the μSR measurements provided the first direct evidence for the spatially inhomogeneous ordered moment size in a perturbed spin gap system.

4 Dynamic relaxation functions for gaussian fields

4.1 Brownian motion of the phase and the SCA

To understand the role of fluctuating random local fields, let us start with a simple model, where a local field H with magnitude $\omega_o = \gamma_\mu H$ alternates its direction between $\hat{\mathbf{x}}$ and $-\hat{\mathbf{x}}$, perpendicular to the initial muon spin polarisation along $\hat{\mathbf{z}}$. After the correlation time τ, the direction of the field is chosen from the two opposite directions randomly with equal probability, having a time evolution such as $++-+---+-++-$ or so on. This will lead to a Brownian motion of the phase of the muon spin precession around H. Each single step of this Brownian motion proceeds with the phase $\omega_0\tau$. After time t, there exist $N = t/\tau$ steps of motion. The deviation from the initial phase is given as $\theta(t) = \sqrt{N} \times \omega_0\tau = \sqrt{t} \times \sqrt{\tau} \times \omega_0$ Then we can obtain the relaxation time "T_1" when the deviation of the phase becomes 1 radian as $T_1 = 1/(\omega_0^2\tau)$, or better known as the relaxation rate $1/T_1 \propto \omega_0^2\tau = \omega_0^2/\nu$, where $\nu = 1/\tau$ denotes the fluctuation rate of random local fields. This approximation works for the "narrowing limit" where $\omega_0\tau \ll 1$. A larger fluctuation rate ν means better averaging of the randomness of the field, and thus resulting in smaller relaxation rate $1/T_1$.

The strong collision approximation (SCA)

A somewhat better description can be obtained by the strong collision approximation (SCA). Here one assumes that the local field changes its direction at a time t which has a probability distribution $\rho(t) \propto \exp(-\nu t)$. The field after such a "collision" is chosen randomly, with no correlation to the field before the collision, from the probability distribution $P(H)$. Let us consider the case for a Gaussian distribution $P^G(H)$ in zero external field. A schematic view of the time evolution of average muon polarisation in this model is illustrated in Figure 13 (Uemura 1982). Until the first collision, the polarisation would decay following the Kubo-Toyabe function. After the collision at $t = t_1$, the spin ensemble will decay, following the Kubo-Toyabe form with $t = t_1$ as the initial time zero. The starting asymmetry at $t = t_1$ is $G_z^G(t_1)$. This scenario will repeat for the second collision at $t = t_2$, etc. Mathematically, these operations would lead to

$$G_z^G(t,\nu) = e^{-\nu t}\left[g_z(t) + \nu\int_0^t g_z(t_1)g_z(t-t_1)dt_1 + \nu^2\int_0^t\int_0^{t_2} g_z(t_1)g_z(t_2-t_1)g_z(t-t_2)dt_1dt_2 + \cdots\right], \tag{16}$$

where g_t denotes the static relaxation function. Figure 14 shows this relaxation by SCA for various values of ν/Δ (Hayano *et al.* 1993a, Kubo and Toyabe 1967).

As illustrated in Figure 13, the relaxation function in the dynamic case can be obtained

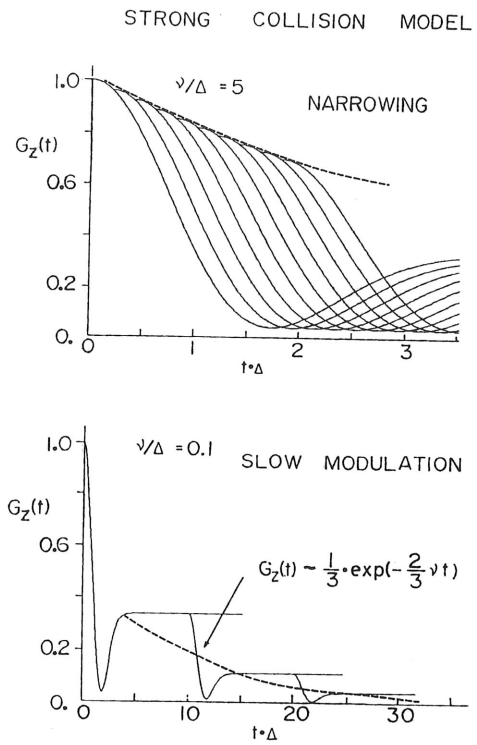

Figure 13. *A schematic view of the time evolution of the average muon spin polarisation in the strong collision approximation for Gaussian random local fields. The dynamic function can be obtained as an envelope of static functions. (Uemura 1982).*

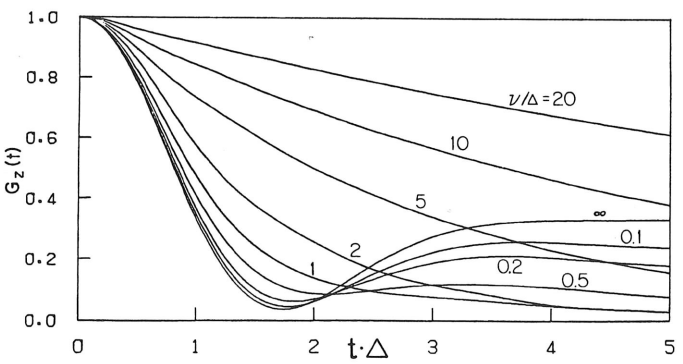

Figure 14. *ZF relaxation function $G_z^G(t, \Delta, \nu)$ obtained by the strong collision approximation (Equation 16) for Gaussian random local fields, plotted for several selected values of ν/Δ (Hayano* et al. *1979b, Kubo and Toyabe 1967).*

as an envelope of those many static functions. This figure demonstrates a few important features. Firstly, the relaxation becomes slower for more collisions, *i.e.* larger ν. Secondly the Gaussian line shape changes into an exponential shape for fast fluctuations $\nu/\Delta \geq 5$. In the limit of fast fluctuations (narrowing limit) the SCA leads to

$$G_z^G(t,\nu) = \exp(-2\Delta^2 t/\nu). \tag{17}$$

It should be noted that SCA works not only for the narrowing limit $\nu/\Delta \gg 1$, but also in the case of slow fluctuations. As shown in Figure 13, the slow fluctuation will cause a decay of the "1/3 tail" of the ZF Kubo-Toyabe function, leading to

$$G_z^G(t,\nu) = (\frac{1}{3})\exp[-(2/3)\nu t]. \tag{18}$$

This feature provides a new method for μSR to probe a very slow dynamic processes in ZF and LF up to its time window of $\sim 10\mu$s, even in systems with large Δ.

4.2 Spectral weight and analytic formula

When local fields are fluctuating with the auto-correlation function

$$\frac{\langle H(0)H(t)\rangle}{\langle H(0)^2\rangle} = \exp(-\nu t), \tag{19}$$

one can make Fourier transformation to obtain a power spectrum in the frequency space $PW(\omega) \propto \nu/(\nu^2+\omega^2)$. The application of LF creates Zeeman levels for muon spins with energy difference $\hbar\omega_L$. Transition between the Zeeman levels occurs with a probability proportional to $\omega = \omega_L$ component of the power spectrum of the field fluctuations $PW(\omega_L)$. Therefore, this dynamic spin flipping process would make the relaxation rate $1/T_1 \propto \nu/(\omega_L^2+\nu^2)$. Combining this with the case of ZF, *i.e.* $\omega_L = 0$, one obtains the relaxation function

$$G_z^G(t,\nu,\omega_L) = \exp[-(2\Delta^2\nu t)/(\omega_L^2+\nu^2)]. \tag{20}$$

This expression is valid only for the narrowing limit $\nu/\Delta \gg 1$, where the relaxation is predominantly caused by the spin flipping. Such a transition between Zeeman levels require exchange of energy with the spin-lattice system, and thus called "spin lattice relaxation" or the "T_1" process. When ν becomes closer to Δ, the spin relaxation reflects both the dephasing process without energy exchange and the dynamic "T_1" process.

Since the gyromagnetic ratio γ_μ is very small, ω_L becomes 85.1MHz for the LF of $H_L =$ 1 kG. This value is much smaller than typical fluctuation rates in solids, ranging between $\nu = 10^{13} - 10^9$ /s. Therefore, in most cases, dynamic relaxation rate $1/T_1$ shows only little dependence on LF. This feature makes contrast with the relaxation due to static local field, which is quite sensitive to LF. This difference provides a way to distinguish between static and dynamic depolarisation processes, as illustrated in Figure 15. Figure 6 compares the ZF and LF relaxation functions in a CuMn spin glass (Uemura *et al.* 1981) at $T \sim 0.5T_g$ and $T > T_g$, which demonstrates that the former (latter) case with predominantly static (dynamic) fields shows a large (small) dependence on LF.

Relaxation functions obtained in SCA have analytic forms only in some few selected limits. It is especially difficult to calculate Equation 16 in the region $\nu/\Delta \sim$1–5. An

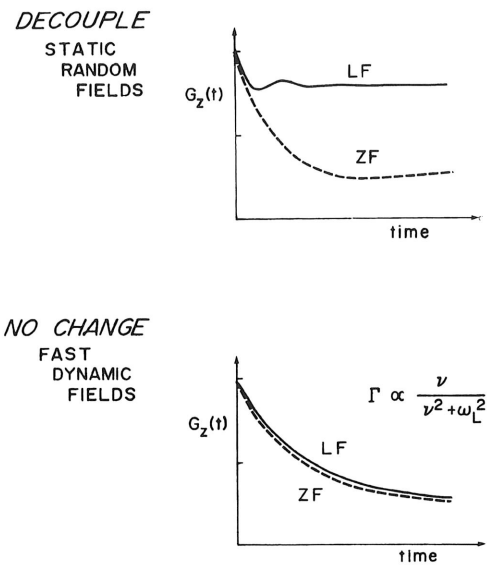

Figure 15. *An illustration of the different dependence of LF between depolarisation due to static and dynamic random local fields. Usually, relaxation caused by static random local fields can easily be "decoupled" by the application of LF (for $\omega_L \gg \Delta$), while the dynamic relaxation with $\nu/\omega_L \gg 1$ and $\nu/\Delta \gg 1$ exhibits little dependence on LF.*

approximate analytic form to cover this region was first given by Abragam (for NMR lineshape arguments) in the case corresponding to the TF relaxation function as

$$G_x^G(t,\nu) = \exp\left[-(\Delta^2/\nu^2) \times \{e^{-\nu t} - 1 + \nu t\}\right], \tag{21}$$

which is commonly called the "Abragam formula" (Abragam 1961). This formula gives the result very close to those in SCA for TF obtained with $g(t) = \exp(-\Delta^2 t^2/2)$, yielding $G_x^G(t,\nu) = \exp(-\Delta^2 t/\nu)$ in the limit $\nu/\Delta \gg 1$.

On should, however, be careful that in the true narrowing limit, the TF relaxation function and ZF relaxation function should have the same decay rate, rather than the factor of 2 difference between the above formula and Equation 17. The SCA process for the TF relaxation function contains only the "adiabatic" or dephasing part of the relaxation due to the random broadening of applied field via one ($i = x$) component of the local field. An additional process which destroys the spin polarisation can be found in transitions between two muon Zeeman levels, which exist in TF as well. The efficiency of this in destroying the phase memory of muon spins is half of that in LF, since a spin flip corresponds to a loss of polarisation to zero in TF while transition to the opposite polarisation in LF. Adding this "non-adiabatic" broadening, the TF relaxation function becomes the same as in ZF or LF (*i.e.* Equation 17) in the limit of $\nu/\Delta \gg 1$ and $\nu/\omega_L \gg 1$. In NMR, this feature is known as the equivalence of $1/T_1$ and $1/T_2$ in the narrowing limit (Abragam 1961,Slichter 1963).

Recently, Keren (1994) obtained a very useful analytic approximate formula for ZF

and LF relaxation functions as

$$G_z(t, \nu, \omega_L) = \exp[-\Gamma(t)\, t],$$

where

$$\Gamma(t)\, t = \frac{2\Delta^2}{(\omega_L^2+\nu^2)^2}\left[(\omega^2+\nu^2)\nu t + (\omega_L^2-\nu^2)\{1 - e^{-\nu t}\cos(\omega_L t)\} - 2\nu\omega_L e^{-\nu t}\sin(\omega_L t)\right]. \tag{22}$$

This Keren equation gives $\Gamma(t)t = 2(\Delta^2/\nu^2)\{e^{-\nu t}-1+\nu t\}$ similar to the Abragam formula (Equation 21) with a factor of 2 larger rate in zero field ($\omega_L \to 0$), while Equation 20 for the narrowing limit $\nu/\Delta \gg 1$. Keren compared this function with the SCA results and with numerical Monte-Carlo results, and demonstrated good agreements as shown in Figure 16.

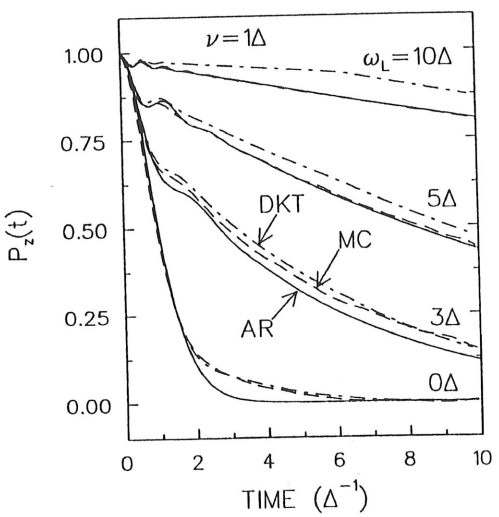

Figure 16. *Comparison of ZF and LF relaxation functions obtained in the strong collision approximation (DKT), Monte-Carlo simulation (MC) and analytic approximation (Equation 22) by Keren (AR) (Keren 1994).*

5 $1/T_1$ data in an itinerant weak-ferromagnet MnSi

ZF and LF μSR measurements to study $1/T_1$ in magnetic systems started at TRIUMF in 1978 with MnO (Hayano 1978a) and MnSi (Hayano 1978b). Here we shall look into the case of MnSi. MnSi is a weak ferromagnet (more precisely having a long period helical spin structure) based on itinerant electrons, with $T_c \sim 30K$ and a rather reduced ordered moment size of $\sim 0.4\mu_B$/Mn (Motoya 1978,Ishikawa 1976). The ZF- and LF-μSR results in MnSi at room temperature was shown in Figure 4. The fluctuation of electron spins are so fast at this temperature that the $1/T_1$ relaxation is invisible. This allowed us to study nuclear dipolar fields. When cooled down closer to T_c, the dynamic relaxation becomes

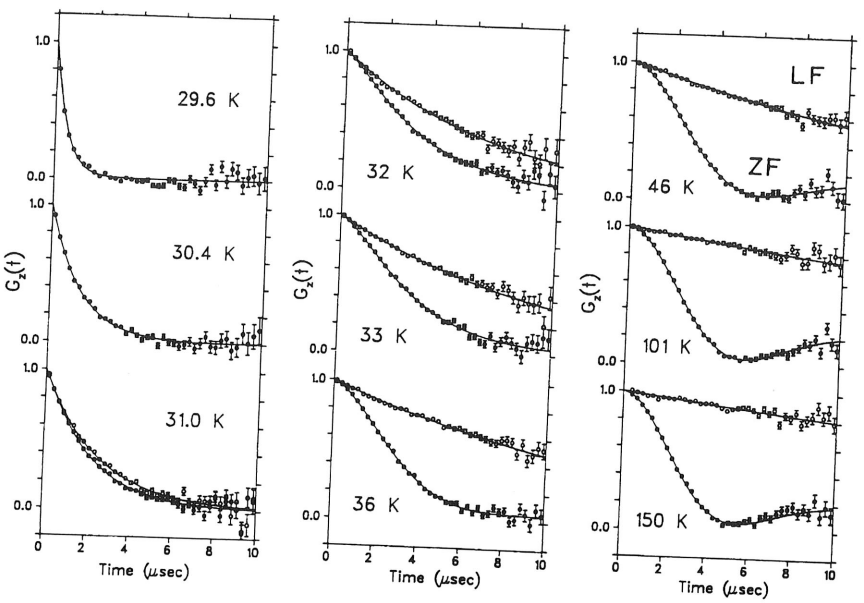

Figure 17. *Muon spin relaxation functions observed in MnSi with ZF and LF = 122G. The results in LF show the dynamic relaxation function due to itinerant electrons, while those in ZF are obtained as a product of that dynamic function with a quasi-static relaxation function due to nuclear dipolar fields from ^{55}Mn nuclei. The decay of the 1/3 tail of the quasi-static Kubo-Toyabe relaxation function is caused by a slow fluctuations of ^{55}Mn nuclei, which are subject to the nuclear $1/T_1$ process with spins of itinerant electrons (Kadona* et al. *1990).*

visible. Figure 17 shows the temperature dependence of the relaxation functions observed in ZF and LF = 122G in a rather recent measurements of MnSi (Kadona *et al.* 1990). When static nuclear dipolar fields co-exist with dynamic random local fields from electron spins, the relaxation function is given as a product of the static and dynamic functions. The applied LF is enough to make the static function for nuclear dipolar fields to be close to 1, thus allowing a selective observation of the $1/T_1$ relaxation due to electron moments.

In the original study by Hayano *et al.* (1978a), $1/T_1$ was observed in LF = 700G. The temperature dependence of T_1 is shown in Figure 18, which demonstrates that $1/T_1 \propto T/(T - T_c)$ above T_c. Relaxation rate of a magnetic probe can be related to generalised susceptibility (Moriya 1963) as

$$1/T_1 \propto k_B T \sum_q \mathrm{Im}\,[\chi_\perp(q, \omega_L)]/\omega_L, \tag{23}$$

where $\chi_\perp$ represents the component perpendicular to the direction of external LF. Moriya (1985) developed the self-consistent renormalisation (SCR) theory to describe the behaviors in itinerant electron magnets, overcoming difficulties in the Hartree Fock-random phase approximation method. The SCR theory explains the observed Curie-Weiss behavior of uniform susceptibility $\mathrm{Re}\,[\chi(q = 0)] \propto 1/(T - T_c)$, reduced ordered moment size, reduced transition temperature, etc. The SCR theory predicts $1/T_1 \propto T/(T - T_c)$ for weak-ferromagnets: the numerator represents usual Korringa relation for simple metals,

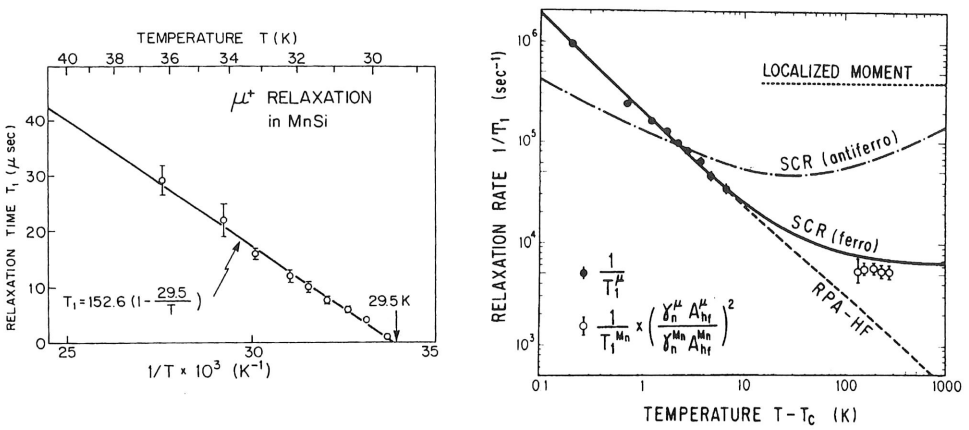

Figure 18. *(a) Temperature dependence of the relaxation time T_1 of muon spins observed in MnSi with LF=700G, and (b) the relaxation rate $1/T_1$ from μSR compared with theoretical predictions and with $1/T_1$ of ^{55}Mn NMR (Hayano* et al. *1978a).*

while the denominator represents the Curie-Weiss susceptibility for $q = 0$ where dynamic susceptibility has a dominant contribution. As shown in Figure 18, the observed relaxation rate in MnSi agrees well with this prediction of SCR theory.

Let us consider a crossover from a localised moment magnet (such as EuO) to an itinerant ferromagnet (Fe, Ni) to a weak-itinerant ferromagnet (MnSi) to a non-magnetic metal (Al). In inelastic neutron scattering studies, the intensity at $T > T_c$ ranges in the energy scale of $J \sim kT_c$ in EuO, while increasingly higher higher energy scales with respect to kT_c from Ni (Uemura *et al.* 1983) to MnSi (Ishikawa *et al.* 1985), and finally to the Fermi energy in Al (Uemura *et al.* 1984). This large energy scale of excitable states in MnSi leads to changes of the relaxation rate over a wide temperature range. In contrast, $1/T_1$ in the paramagnetic state of localised moment systems usually does not depend on T, except for the narrow critical region, since the exchange fluctuation with $\nu \propto J/h$ is not a thermal process. This difference is illustrated in Figure 18.

In MnSi, NMR measurements of ^{55}Mn can observe $1/T_1$ only at high temperatures (Yasuoka *et al.* 1978), restricted by the initial dead time of the NMR spin echo method. Figure 18 shows that the μSR results can be connected nicely with those from NMR, after making correction for different hyperfine coupling constants of μ^+ and ^{55}Mn. In the temperature range between T = 32 and 100K, the relaxation time T_1 of ^{55}Mn comes into the time range of 1-10 μs. Then, this nuclear T_1 process leads to the nuclear dipolar field from ^{55}Mn to fluctuate, and changes the Kubo-Toyabe line shape. Such a change is shown in Figure 17, which demonstrates that the "1/3 tail" of the Kubo-Toyabe function starts to decay around T = 100K. This feature allows detecting $1/T_1$ of Mn nuclei via muon spin relaxation, as a kind of "double resonance" method (Kadona 1990).

The $1/T_1$ relaxation rate of μ^+ can also be measured below T_c through a decay rate of the 1/3 asymmetry. One can also measure the temperature dependence of the (sublattice) magnetisation via the observed muon spin precession frequency. Figure 19 shows these results below T_c obtained in MnSi (Takigawa 1980).

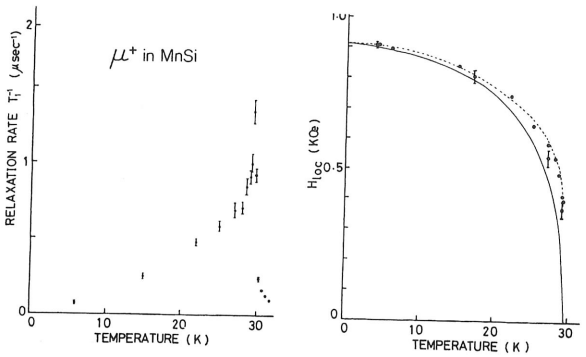

Figure 19. *Dynamic muon spin relaxation rate* $1/T_1$ *and the precession frequency* ν_μ *observed by ZF-*μ*SR in MnSi below* T_c *(Takigawa* et al. *1980).*

6 Dynamic relaxation functions for Lorentzian fields

6.1 Spatial average and dynamicisation

When we adopt the SCA formula of Equation 16 with the static function of Equation 7 to calculate dynamic relaxation function for Lorentzian local fields, we obtain the results shown in Figure 20, which exhibits no change of the initial decay rate even for very fast

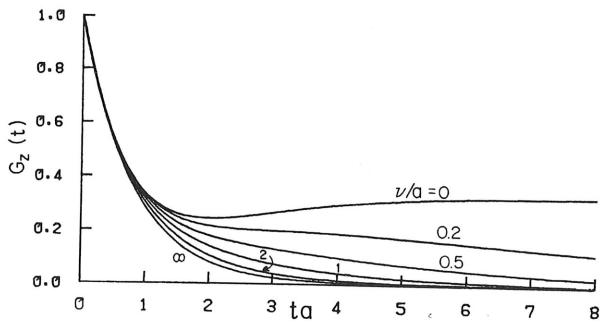

Figure 20. *Muon spin relaxation function obtained when the strong collision approximation is adopted with* $G_z^L(t)$ *of Equation 7 as the static function* $g(t)$ *in Equation 16. There is no change of the damping rate even for a rather fast fluctuation rate* $\nu/a \gg 1$ *(Uemura 1982).*

fluctuations $\nu/a \gg 1$. This occurs because the envelope function of multiple functions in Figure 13 becomes the exponential static function itself. On the other hand, the observed data in a dilute alloy spin glass AuFe in Figure 21 definitely shows the reduction of the relaxation rate with increasing temperature, presumably due to faster fluctuations of Fe moments.

This apparent contradiction can be resolved when we notice that different muon sites have different variable ranges of local fields, as illustrated in Figure 22. When local field at a muon site undergoes a dynamic fluctuation, the field after this "collision" is chosen

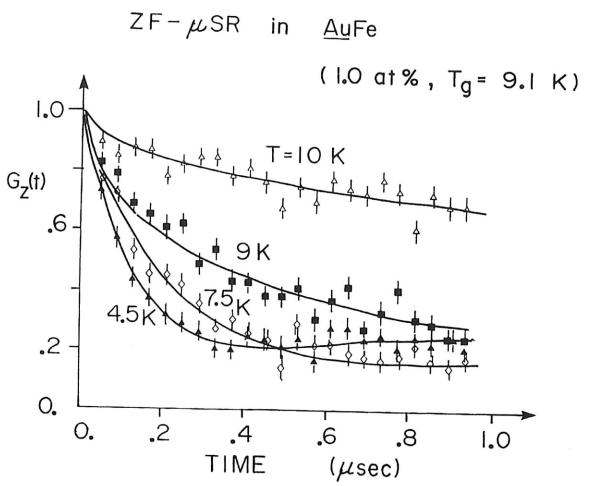

Figure 21. *ZF-μSR spectra observed in a dilute-alloy spin glass AuFe (Fe 1.0 at.%; $T_g = 9.1K$) (Uemura* et al., *1980, 1985).*

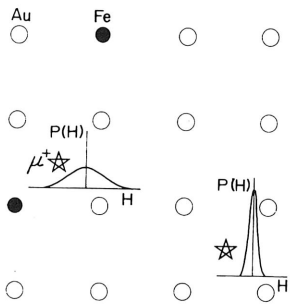

Figure 22. *Schematic view of different variable ranges of random local fields at different muon sites in dilute-alloy spin glasses. When Fe moments fluctuate, the local field at a muon site closer to the magnetic ions will be modulated in a wider range (Uemura* et al. *1985, Uemura 1982).*

from the variable range of random fields associated to the particular muon site. For simplicity, we shall approximate such a "sub-distribution" of fields at each j-th muon site by a Gaussian distribution P_j^G with the width Δ_j. The probability $\rho(\Delta_j)$ to find a site with Δ_j should satisfy

$$P^L(H_i) = \int_0^\infty P^G(H_i \Delta_j)\rho(\Delta_j)d\Delta_j \qquad (24),$$

so that we recover the overall Lorentzian distribution. Equation 24 leads to

$$\rho(\Delta) = \sqrt{(2/\pi)} \times (a/\Delta^2) \times \exp(-a^2/2\Delta^2). \qquad (25)$$

Using this sub-distribution, Uemura *et al.*(1980, 1985) derived ZF relaxation functions for

dynamic Lorentzian fields with a single fluctuation rate ν as

$$G_z^L(t,a,\nu) = \int_0^\infty G_z^G(t,\Delta,\nu)\rho(\Delta)d\Delta. \tag{26}$$

Figure 23 shows these functions for various values of ν/a. We notice that now $G_z^L(t,a,\nu)$

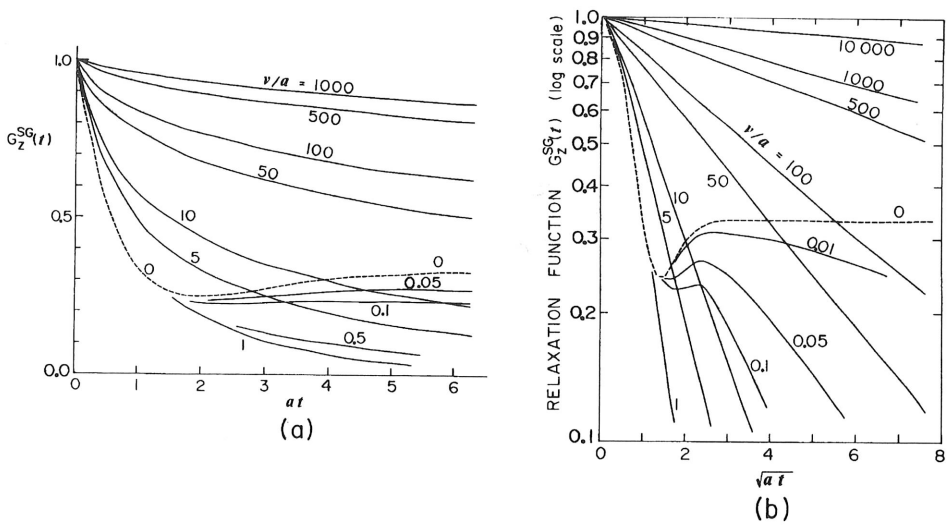

Figure 23. *(a) Muon spin relaxation function in ZF for Lorentzian random local fields with the strong collision approximation, obtained by taking into account the different variable ranges of local fields at different muon sites with the spatial averaging of Equation 26. (b) shows the same function in a plot of* $\ln[G(t)]$ *versus* $\sqrt{at}$. *This figure demonstrates the square-root exponential time dependence of* $G_z^L(t)$ *(Equation 27) for fast fluctuations* $\nu/a \gg 1$ *(Uemura* et al., *1980, 1985).*

depends on the fluctuation rate ν. This example demonstrates the importance of order of two operations, dynamicisation and spatial average, in random systems. Reversing the order ends up in a completely different results, Figures 21 and 23.

In the narrowing limit, Equation 26 reduces to (Uemura 1982, Uemura *et al.* 1985)

$$G_z^L(t,a,\nu) = \exp\left(-\sqrt{4a^2t/\nu}\right). \tag{27}$$

The stretched exponential form originates from averaging exponential functions with different decay rates $1/T_1$, corresponding to different magnitudes Δ_j of random local fields. This time dependence is well illustrated in Figure 23 (b), which plots $\ln G_z^L(t,a,\nu)$ versus $\sqrt{at}$. The experimental data obtained in AuFe in

Figure 24 clearly shows this square-root time dependence, as demonstrated by the straight lines at $T > T_g = 9.1$K (Uemura *et al.* 1985).

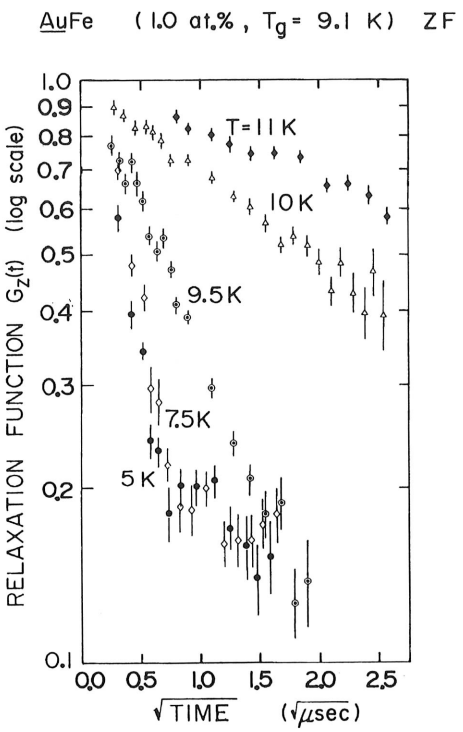

Figure 24. *Zero-field muon spin relaxation function observed in AuFe (Fe 1.0 at.%; $T_g = 9.1K$), plotted in* $\ln[G(t)]$ *versus* $\sqrt{t}$. *The results above T_g follow straight lines corresponding to root-exponential decay. Those below T_G show initial fast relaxation followed by a slow decay, similar to the theoretical calculation for co-existing static and dynamic local fields shown in Figure 25 (Uemura* et al. *1985).*

6.2 Coexisting static and dynamic fields

Below the susceptibility cusp temperature T_g, Fe or Mn spin S in these spin glasses is considered to acquire a static polarisation along a direction attached to each individual moment. The auto correlation function for a spin S_j in this situation can be given as

$$\frac{\langle S_j(t)S_j(0)\rangle}{\langle S_j(0)^2\rangle} = (1-Q)e^{-\nu t} + Q, \tag{28}$$

where Q is often called Edwards-Anderson order parameter (Edwards and Anderson 1975,1976). Let us assume that the correlation function of the local field H is also given by the above formula. The corresponding μSR relaxation function for $\nu/a \gg 1$ can be obtained by first calculating

$$G_z^G(t,\Delta,\nu,Q) = [G_z^G(t,\Delta_s)] \times \exp(-2\Delta_d^2 t/\nu);$$
$$\Delta_s^2 = Q \times \Delta^2; \quad \Delta_d^2 = \Delta^2 - \Delta_s^2, \tag{29}$$

where Δ_s and Δ_d represent effective amplitude of static and dynamic local fields. Multiplying static and dynamic functions is a standard procedure when static and (fast) dynamic fields coexist at a muon site.

We then have to make a spatial average of Equation 29 over $\rho(\Delta_j)$ as in Equation 26. This spatial averaging leads to an analytic form (Uemura 1982, Uemura *et al.* 1985)

$$G_z^L(t) = \frac{1}{3}\exp\left(-\sqrt{4a_d^2 t/\nu}\right) + \frac{2}{3}\left[1 - \frac{a_s^2 t^2}{\sqrt{(4a_d^2 t/\nu) + a_s^2 t^2}}\right]\exp\left(-\sqrt{(4a_d^2 t/\nu) + a_s^2 t^2}\right);$$

with

$$a_s^2 = Q \times a^2; \qquad a_d^2 = a^2 - a_s^2, \tag{30}$$

where a_s and a_d denote static and dynamic amplitudes of Lorentzian random fields. The effect of onset of static order parameter Q in this function is shown in Figure 25, which exhibits various characteristic features found in the data of Figure 24 below $T_g = 9.1$K.

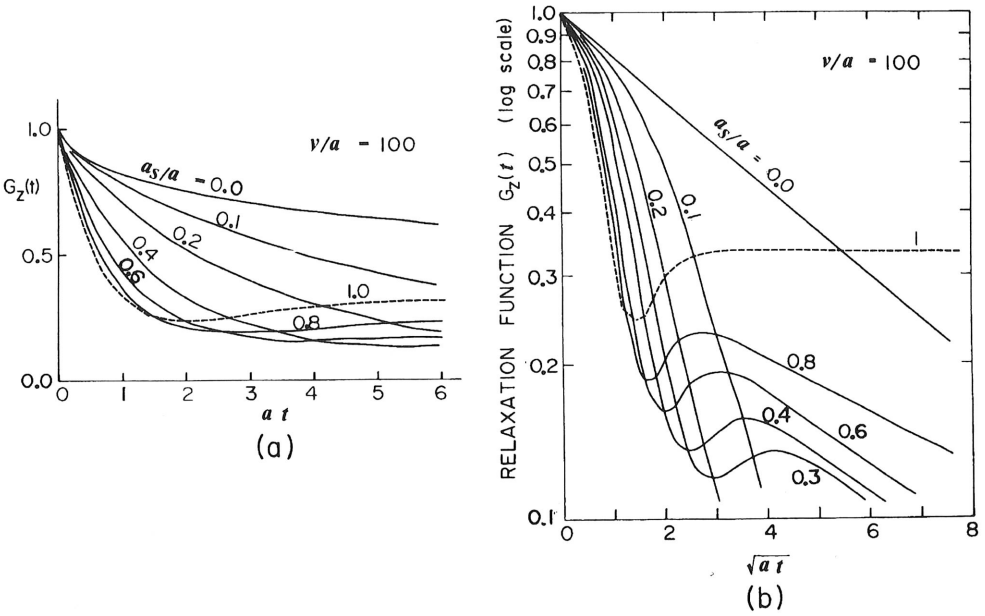

Figure 25. *ZF muon spin relaxation function of Equation 30 calculated for coexisting static and dynamic random local fields at each muon site, with dynamic modulation rate* $\nu/a = 100$ *for various static amplitudes* a_s. *The increasing static amplitude of random fields causes increasingly quick initial decay of* $G_z(t)$ *followed by the slowly damping "tail", having the relaxation rate comparable to the paramagnetic case with* $a_s/a = 0$ *(Uemura* et al. *1985).*

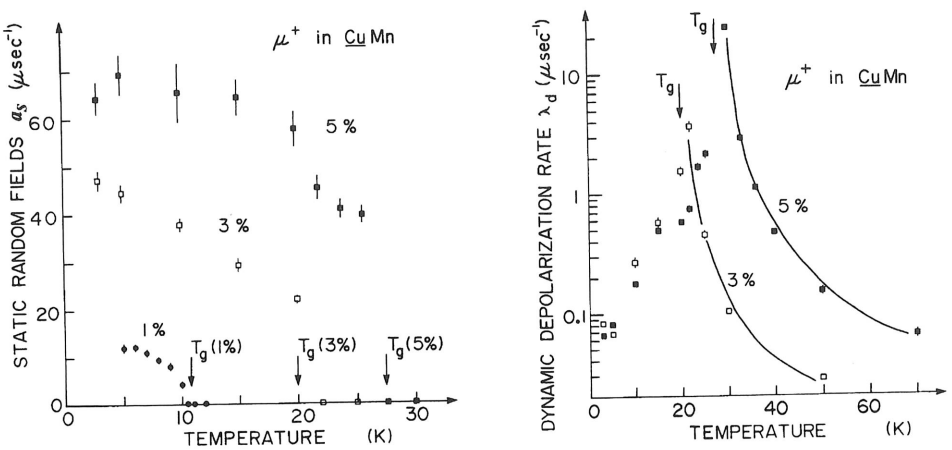

Figure 26. *(a) The static amplitude a_s of random local fields and (b) the dynamic depolarisation rate λ_d in CuMn spin glasses, determined by fitting the observed ZF-μSR spectra with Equation 30. To account for nuclear dipolar fields from Cu nuclei, we multiplied Equation 30 with the Kubo-Toyabe function for pure Cu if a_s is smaller than $\Delta_{Cu} \sim 0.3\mu s^{-1}$. The static amplitude a_s becomes finite only below T_g for all the CuMn samples, and the linear dependence of the static random fields at $T \to 0$ on the Mn concentration is demonstrated in (a) (Uemura* et al. *1985).*

6.3 Results in dilute alloy spin glasses AuFe and CuMn

Figure 26 shows the temperature dependences of the static amplitude parameter a_s and of the dynamic relaxation rate $\lambda_d \equiv 4a_d^2/\nu$ obtained by fitting the observed μSR results in CuMn spin glasses (Uemura *et al.* 1985) with Equation 26 and Equation 30. Figure 6 shows the results for a_s in AuFe. The static amplitude appears below the cusp temperature T_g, and increases towards the full amplitude a_0, calculated theoretically from the size of Fe/Mn moments and its concentration. The μSR results of a_s in AuFe are compared with the static field observed by the Mössbauer effect (Violet and Borg 1965) in Figure 27, which shows a reasonable agreement of the results from these two techniques.

The dynamic relaxation rate in Figure 26 shows a divergent increase around T_g approached both from above and below T_g. The fluctuation rate ν of Mn/Fe moments derived from the observed relaxation rate λ_d above T_g is plotted in Figure 28. This figure demonstrates a critical slowing down of Mn/Fe moments occurring over a wide rage of temperature $T = T_g - 2T_g$ with a wide range of fluctuation rate 10^{12}–10^8/s.

Neutron spin echo (NSE), invented by Mezei (1982), is an ingenious technique for inelastic neutron scattering with a very high energy resolution which allows direct observation of the time correlation function of spins. In Figure 28, we plotted the average decay rate of spin fluctuations observed by NSE (Mezei and Murani 1979), which agree reasonably well with the μSR results. Static spin polarisation of spin glasses can be measured also by ac-susceptibility χ_{ac}, at the time window of the measuring ac frequency. ZF-μSR provides dynamic and static information via the fluctuation rate ν and the static amplitude a_s corresponding to the time window of $\sim 10^{-7}$–10^{-6}s. We performed μSR

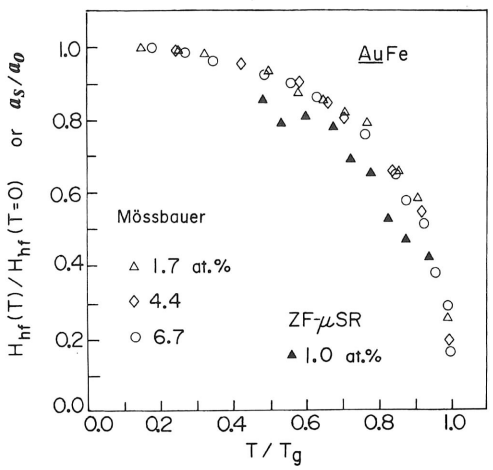

Figure 27. *Comparison of the static random local fields a_s/a_0 observed in ZF-μSR in AuFe (1.0 at.%) with the static hyperfine field H_{hf} measured by ^{57}Fe Mössbauer effect experiments in various AuFe specimens by Violet and Borg (1965) (data from Uemura* et al. *1985).*

measurements using the same specimen of 5at% CuMn spin glass that was used in the NSE (Mezei and Murani 1979) and the χ_{ac} (Tholence 1980) measurements. The results from all these three experiments are combined in Figure 29 which shows the correlation function of Cu spins in the time range of 10^{-12}–10^{-2}s. The combined results demonstrate a slowing down of Cu spin fluctuations above $T_g = 27.4$K, and the appearance of a persisting static order parameter below T_g. This figure also demonstrates the complementary time windows of these three different experimental probes.

6.4 Stretched exponential relaxation functions

In more recent measurements of dilute and concentrated spin glass systems (Campbell*et al.* 1994, Keren *et al.* 1996), a stretched exponential form of the relaxation function

$$G_z(t) = \exp[-(\lambda t)^{\beta}], \tag{31}$$

was observed with the power β different from 1 or 1/2. The power β in several systems approaches 1/3 near T_g from values close to 1 (or 1/2 in dilute alloys) at high temperatures, as shown in Figure 30. We can consider a few different origins for this 1/3 power. We obtained the square-root relaxation function (Equation 27) by assuming that Mn/Fe moments are fluctuating with a single fluctuation rate ν. When spatial distribution of ν is taken into account, the power β for the dilute limit becomes smaller than 1/2. In the limit of large variable range of ν, a numerical study (Merrin and Uemura, unpublished) gives a power close to 1/3. We can also consider violation of Markovian process as another possible origin of deviation from $\beta = 1/2$. This possibility is discussed by Campbell in the accompanying lecture (Campbell 1998). The time correlation function of Mn moments observed by NSE in a CuMn spin glass shows a non-exponential decay

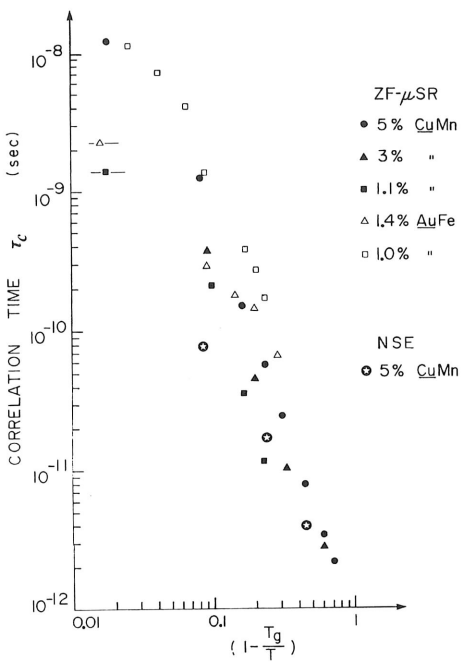

Figure 28. *The correlation time $\tau_c \equiv 1/\nu$ of Mn (or Fe) moments determined by ZF-μSR results using the dynamic relaxation rate in Figure 26 observed above T_g. The results from different specimens are plotted against the reduced temperature $(1 - T/T_g)$ of each specimen. A straight line corresponds to a power law of critical slowing down. Also plotted is a time $\tau_{\rm NSE}$ when the time correlation function of Mn moments in CuMn (5 at.%) measured by neutron spin echo decays to $1/e$ (Uemura* et al. *1985).*

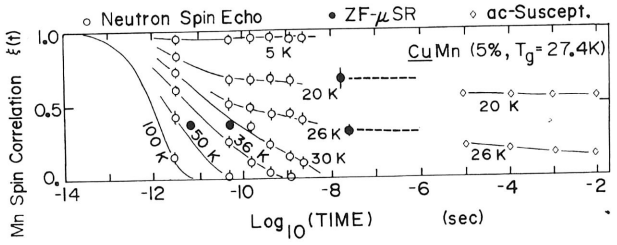

Figure 29. *Comparison of the time correlation function $\xi(t)$ of the Mn moment in CuMn (5 at.%) measured by neutron spin echo (Mezei and Murani 1979), ZF-μSR, and ac-susceptibility $\chi_{\rm ac}$ (Tholence 1980). The triangle points for ZF-μSR are plotted at $\xi(t = \tau_c) = 1/e$ at T=50K and 36K (above $T_g = 27.4K$), and at $\xi(t = \tau_c) = (1 - Q)/e + Q$ with $Q = (a_s/a_0)^2$ at T=26K and 20K. The solid circles are plotted to represent the static polarisation at $\xi(t = 1/a_s) = (a_s/a_0)^2$ at T=26K and 20K, and the attached dashed lines indicate the persistency of this polarisation expected from the characteristic "tail" of $G_z(t)$ observed in ZF-μSR (Uemura* et al. *1985).*

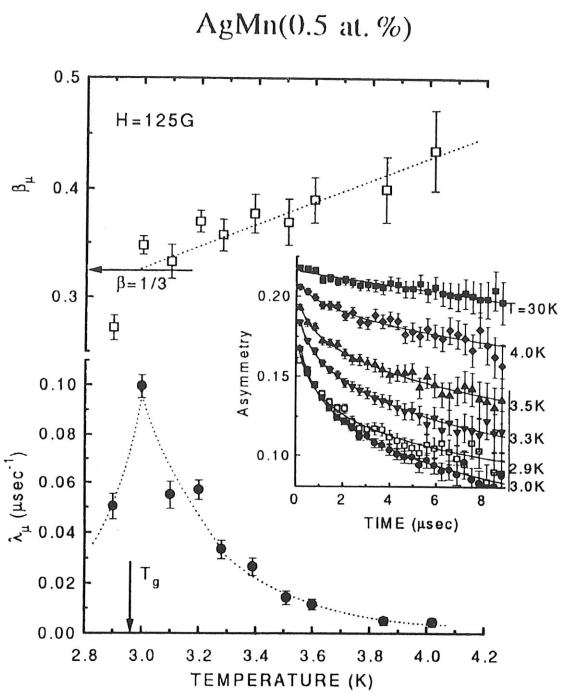

Figure 30. *Temperature dependence of the dynamic relaxation rate λ_d and the power β obtained by fitting the ZF-μSR results in AgMn (0.5 at.%) with the stretched exponential relaxation function Equation 31 shown with the observed ZF-μSR spectra at several temperatures (Keren 1966).*

above T_g in Figure 29. This could be related to spatial averaging of different exponential decays or non-Markovian dynamics of each Mn moment or both.

The stretched exponential relaxation function was observed also in the colossal magnetoresistance system (La,Ca)MnO_3 (Heffner *et al.* 1996). In this case, spin dynamics related to a formation of magnetic polaron may cause inhomogeneous distribution of the fluctuation rate ν in the system, leading to the stretched exponential form.

7 Conclusions

We have provided an overview of relaxation functions observed by μSR in various magnetic systems. With the advent of meson facilities and instrumentation, one can now study rather detailed features of spin systems via analyses of lineshapes of the relaxation functions. Although we have not covered much in this article, many μSR studies have been and will be performed in various new magnetic systems, such as geometrically frustrated and/or low dimensional spin systems, re-entrant spin glasses, doped and undoped spin-gap systems, etc. μSR studies in these new systems may reveal yet more interesting and novel features of relaxation functions.

Acknowledgement

The author would like to thank T. Yamazaki, M.I. Larkin, A. Keren, K. Kojima and J. Merrin for discussions on relaxation functions, and S. Kilcoyne, R. Cywinski and S. Lee for their hospitality during the SUSSP summer school at St. Andrews. This work is supported by a grant from NSF (DMR 98-02000).

References

Abragam A, 1961, *The principles of nuclear magnetism*, (Oxford University Press, Oxford).

Brewer J H, Crowe K M, Gygax F N and Schenck A, 1975, Positive muons and muonium in matter, i*Muon Physics III* (Academic Press, New York), editors Hughes V W and Wu C S.

Campbell I M, Lecture this volume 1998.

Campbell I A, Amato A, Gygax F N, Herlach D, Schenck A, Cywinski R and Kilcoyne S H, 1994, *Phys. Rev. Lett.* **72** 1291.

Chow K H, Pattenden P A, Blundell S J, Hayes W, Pratt F L, Jestädt Th,Green M A, Millburn J E, Rossinsky M J, Hitti B, Dunsiger SR, Kiefl R F, Chen C and Chowdhry A J S, 1996, *Phys. Rev. B* **53** R14725.

Crook M R and Cywinski R, 1997, *J. Phys.: Condens. Matter* **9** 1149.

Edwards S F and Anderson P W, 1975, *J. Phys. F* **5** 965.

Edwards S F and Anderson P W, 1976, *J. Phys. F* **6** 927.

Foy M L G, Heiman N, Kossler W J and Stronach C E, 1973, *Phys. Rev. Lett.* **30** 1064.

Fukuyama H, Tanimoto T and Saito M, 1996, *J. Phys. Soc. Japan* **65** 1182.

Graf H, Hofman W, Kündig W, Meier P F, Patterson B D and Rodoriguez A, 1978, *Solid State Commun.* **25** 1079.

Hase M, Terasaki I, Sasago Y, Uchinokura K and Obara H, 1993, *Phys. Rev. B* **71** 4059.

Hase M, Terasaki I and Uchinokura K, 1993, *Phys. Rev. Lett.* **70** 3651.

Hayano R S, Uemura Y J, Imazato J, Nishida N, Nagamine K, Yamazaki T and Yasuoka H, 1978a, *Phys. Rev. Lett.* **41** 421.

Hayano R S, Uemura Y J, Imazato J, Nishida N, Yamazaki T, Yasuoka H and Ishikawa Y, 1978b, *Phys. Rev. Lett.* **41** 1743.

Hayano R S, Uemura Y J, Imazato J, Nishida N, Yamazaki T and Kubo R, 1979, *Phys. Rev. B* **20** 850.

Heffner RH, Le L P, Hundley M F, Neymeier J J, Luke G M, Kojima K, Nachumi B, Uemura Y J, MacLaughlin D E and Cheong S W, 1996, *Phys. Rev. Lett.* **77** 1869.

Ishikawa Y, Tajima K, Bloch D and Roth M, 1976, *Solid State Commun.* **19** 525.

Ishikawa Y, Noda Y, Uemura Y J, Majkrzak C F and Shirane G, 1985, *Phys. Rev. B* **31** 5884.

Jaccarino V, 1965, Nuclear resonance in antiferomagnets, in *Magnetism II A*, (Academic Press, New York) editors Rado G T and Suhl H.

Kadono R, Matsuzaki T, Yamazaki T, Kreitzman S R and Brewer J H, 1990, *Phys. Rev. B* **42** 6515.

Keren A, 1994, *Phys. Rev. B* **50** 10039.

Keren A, Mendels P, Campbell I A and Lord J, 1996, *Phys. Rev. Lett.* **77** 1386.

Kojima K, Fudamoto Y, Larkin M, Luke G M, Merrin J, Nachumi B, Uemura Y J, Hase M, Sasago Y, Uchinokura K, Ajiro Y, Revcolevschi A and Renard J P, 1997, *Phys. Rev. Lett.* **79** 503.

Kubo R, 1981, *Hyperfine Interact.* **8** 731.

Kubo R and Toyabe T, 1967, *Magnetic Resonance and Relaxation* p.810. (North-holland, Amsterdam), editor Blinc R.

Le L P, Keren A, Luke G M, Sternlieb B J, Wu W D, Uemura Y J, Brewer J H, Riseman T M, Upasani R V, Chiang L Y, Kang W, Chaikin P M, Csiba T and Grüner G, 1993, *Phys. Rev.B* **48** 7284.

Le L P, Heffner R H, Thompson J D, Nieuwenhuys G J, MacLaughlin D E, Canfield P C, Cho B K, Amato A, Feyerherm R, Gygas F N and Schenck A, 1997, *Hyperfine Interact.* **104** 49.

Luke G M, Fudamoto Y, Gingras M J P, Kojima K M, Larkin M, Merrin Nachumi J B and Uemura Y J,1998, *J. Mag. Mag. Matrs.* **177-181** 754; and unpublished results.

Luke G M, Le L P, Sternlieb B J, Wu W D, Uemura Y J, Brewer J H, Riseman T M, Isibashi Sand Uchida S,1991, *Physica C* **185-189** 1175.

Manabe K, Ishimoto H, Koide N, Sasago Y and Uchinokura K, 1998, *Phys. Rev. B* **58** R575.

Mezei F, 1982, Proceedings of a Workshop on Neutron Spin Echo, *Springer Lecture Notes in Physics* **128** (Springer Berlin).

Mezei F and Murani A P, 1979, *J. Mag. Mag. Matrs.* **14** 211.

Moriya T, 1963, *J. Phys. Soc. Japan* **18** 516.

Moriya T, 1985, *Spin Fluctuations in Itinerant Electron Magnetism* (Springer, Berlin), and references therein.

Motoya K, Yasuoka H, Nakamura Y, Jaccarino V and Wernick J H, 1978, *J. Phys. Soc. Japan* **44** 833.

Nachumi B, Fudamoto Y, Keren A, Kojima K M, Larkin M L, Luke G M, Merrin J, Tchernyshyov O, Uemura Y J, Ichikawa N, Goto M, Takagi H, Uchida S, Crawford M K, McCarron E M, MacLaughlin D E and Heffner R H, 1998, *Phys. Rev. B* **58** 8760.

Nishida N, Hayano R S, Nagamine K, Yamazaki T, Brewer J H, Garner D M, Fleming D G, Takeuchi T and Ishikawa Y, 1977, *Solid State Commun* **22** 235.

Shlesinger M F, Zaslavsky G M and Frisch U, 1995, *Lévy Flights and Related Topics in Physics* (plinger , Berlin).

Slichter C P, 1963, *Principles of Magnetic Resonance*, (Harper & Row, New York).

Takigawa M, Yasuoka H, Uemura Y J, Hayano R S, Yamazaki T and Ishikawa Y, 1980, *J. Phys. Soc. Japan* **49** 1760.

Tholence J L, 1980, *Solid State Commun.* **35113,** and private communication.

Uemura Y J, 1982, PhD Thesis, Univ. Tokyo.

Uemura Y J, 1984, Proc. of High Energy Excitations In Condensed Matter Workshop, Los Alamos National Lab. *National Lab. LA-10227-C,* 264-290, editor Silver R N.

Uemura Y J, Yamazaki T, Hayano R S, Nakai R and Huang C Y, 1980, *Phys. Rev. Lett.* **45** 583.

Uemura Y J, Yamazaki T, Harshman D R, Senba M and Ansaldo E J, 1985, *Phys. Rev. B* **31** 546.

Uemura Y J, Hayano R S, Imazato J, Nishida N and Yamazaki T, 1979, *Solid State Commun.* **31** 731.

Uemura Y J, Nishiyama K, Yamazaki T and Nakai R, 1981, *Solid State Commun.* **39** 461.

Uemura Y J, Kossler W J, Yu X H, Kempton J R, Chen H S, Opie D. Stronach C E, Johnston D C, Alvarez M S and Goshorn D P, 1987, *Phys. Rev. Lett.* **59** 1045.

Uemura Y J and Luke G M, 1993, *Physica B* **186-188** 223.

Uemura Y J, Shirane G, Steinsvoll O and Wicksted J P, 1983, *Phys. Rev. Lett.* **51** 2322.

Violet C E and Borg R J, 1965, *Phys. Rev.* **149** 540 .

Walstedt R E and Walker L R , 1974, *Phys. Rev. B* **9** 4857.

Yamazaki T, 1997, *Hyperfine Interact.* **104** 3.

Yasuoka H, Jaccarino V, Sherwood R C and Wernick J H, 1978, *J. Phys. Soc. Japan* **44** 842.